J|A|C|S ARTICLES

Published on Web 04/27/2010

Conductance and Geometry of Pyridine-Linked Single-Molecule Junctions

M. Kamenetska,[†,‡] Su Ying Quek,[§] A. C. Whalley,[∥] M. L. Steigerwald,[‡,∥] H. J. Choi,[⊥] Steven G. Louie,[§,#,▽] C. Nuckolls,[‡,∥] M. S. Hybertsen,[○] J. B. Neaton,*[,§] and L. Venkataraman*[,†,‡]

Department of Applied Physics and Applied Mathematics, Columbia University, New York, New York 10027, Center for Electron Transport in Nanostructures, Columbia University, New York, New York 10027, The Molecular Foundry, Lawrence Berkeley National Laboratory, Berkeley, California 94720, Department of Chemistry, Columbia University, New York, New York 10027, Department of Physics and IPAP, Yonsei University, Seoul 120-749, Korea, Department of Physics, University of California, Berkeley, California 94720, Materials Science Division, Lawrence Berkeley National Laboratory, Berkeley, California 94720, and Center for Functional Nanomaterials, Brookhaven National Laboratory, Upton, New York 11973

Received February 22, 2010; E-mail: jbneaton@lbl.gov; lv2117@columbia.edu

Abstract: We have measured the conductance and characterized molecule−electrode binding geometries of four pyridine-terminated molecules by elongating and then compressing gold point contacts in a solution of molecules. We have found that all pyridine-terminated molecules exhibit bistable conductance signatures, signifying that the nature of the pyridine−gold bond allows two distinct conductance states that are accessed as the gold−molecule−gold junction is elongated. We have identified the low-conductance state as corresponding to a molecule fully stretched out between the gold electrodes, where the distance between contacts correlates with the length of the molecule; the high-conductance state is due to a molecule bound at an angle. For all molecules, we have found that the distribution of junction elongations in the low-conductance state is the same, while in the high-conductance state, the most likely elongation length increases linearly with molecule length. The results of first-principles conductance calculations for the four molecules in the low-conductance geometry agree well with the experimental results and show that the dominant conducting channel in the conjugated pyridine-linked molecules is through the π^* orbital.

1. Introduction

Understanding the effect of metal−molecule contact geometry on transport characteristics of molecular-scale devices is of critical importance for nanoelectronics.[1−3] In recent years, systematic studies of conductance in single-molecule junctions have been made possible by techniques relying on statistical distributions of large numbers of junction measurements.[2,4−7] This method is effective because the affinity of certain chemical link groups for gold allows the metal−molecule−metal junctions to self-assemble in situ, enabling a large number of repeated measurements. Nevertheless, it has been shown that variations in binding geometry from junction to junction are responsible for most of the width of conductance distributions and for the inconsistency in experimental results.[8−11] Studies comparing the variability of conductance measurements with the nature of the linker−gold bond have shown that some end groups form donor−acceptor bonds with undercoordinated gold atoms and bind selectively, yielding reproducible conductance measurements.[2,12,13] In the case of the amine (NH_2) linker, for example, the nitrogen can change its attachment point while maintaining a constant conductance as the junction is elongated because it

[†] Department of Applied Physics and Applied Mathematics, Columbia University.
[‡] Center for Electron Transport in Nanostructures, Columbia University.
[§] The Molecular Foundry, Lawrence Berkeley National Laboratory.
[∥] Department of Chemistry, Columbia University.
[⊥] Yonsei University.
[#] University of California, Berkeley.
[▽] Materials Science Division, Lawrence Berkeley National Laboratory.
[○] Brookhaven National Laboratory.

(1) Lindsay, S. M.; Ratner, M. A. *Adv. Mater.* **2007**, *19*, 23–31.
(2) Venkataraman, L.; Klare, J. E.; Tam, I. W.; Nuckolls, C.; Hybertsen, M. S.; Steigerwald, M. L. *Nano Lett.* **2006**, *6*, 458–462.
(3) Chen, F.; Li, X. L.; Hihath, J.; Huang, Z. F.; Tao, N. J. *J. Am. Chem. Soc.* **2006**, *128*, 15874–15881.
(4) Xu, B. Q.; Tao, N. J. J. *Science* **2003**, *301*, 1221–1223.
(5) Gonzalez, M. T.; Wu, S. M.; Huber, R.; van der Molen, S. J.; Schonenberger, C.; Calame, M. *Nano Lett.* **2006**, *6*, 2238–2242.
(6) Reichert, J.; Ochs, R.; Beckmann, D.; Weber, H. B.; Mayor, M.; von Lohneysen, H. *Phys. Rev. Lett.* **2002**, *88*, 176804.
(7) Haiss, W.; Wang, C. S.; Grace, I.; Batsanov, A. S.; Schiffrin, D. J.; Higgins, S. J.; Bryce, M. R.; Lambert, C. J.; Nichols, R. J. *Nat. Mater.* **2006**, *5*, 995–1002.
(8) Ulrich, J.; Esrail, D.; Pontius, W.; Venkataraman, L.; Millar, D.; Doerrer, L. H. *J. Phys. Chem. B* **2006**, *110*, 2462–2466.
(9) Li, C.; Pobelov, I.; Wandlowski, T.; Bagrets, A.; Arnold, A.; Evers, F. *J. Am. Chem. Soc.* **2008**, *130*, 318–326.
(10) Li, X. L.; He, J.; Hihath, J.; Xu, B. Q.; Lindsay, S. M.; Tao, N. J. *J. Am. Chem. Soc.* **2006**, *128*, 2135–2141.
(11) Haiss, W.; Martin, S.; Leary, E.; van Zalinge, H.; Higgins, S. J.; Bouffier, L.; Nichols, R. J. *J. Phys. Chem. C* **2009**, *113*, 5823–5833.
(12) Kiguchi, M.; Miura, S.; Takahashi, T.; Hara, K.; Sawamura, M.; Murakoshi, K. *J. Phys. Chem. C* **2008**, *112*, 13349–13352.
(13) Park, Y. S.; Whalley, A. C.; Kamenetska, M.; Steigerwald, M. L.; Hybertsen, M. S.; Nuckolls, C.; Venkataraman, L. *J. Am. Chem. Soc.* **2007**, *129*, 15768–15769.

remains bound to an undercoordinated gold atom.[14] However, with pyridines and many other linkers, where multiple conductance signatures are present, questions remain regarding the exact configuration of a metal−molecule−metal junction and its effect on transport.[9,10,15−19]

In this work, we have measured the conductance and determined the junction geometries for the four pyridine-terminated molecules 4,4′-bipyridine (**1**), 1,2-bis(4-pyridyl)ethylene (**2**), 4,4″-bis(4-terpyridine) (**3**), and 1,2-bis(4-pyridyl)ethane (**4**) using the scanning tunneling microscope (STM)-based break-junction technique.[2,4] We have demonstrated that all four molecules exhibit two conducting configurations: molecular junctions start in a high-conductance configuration that can be elongated over a distance that depends on the molecular length[14] and generally terminate with a low-conductance plateau whose length distribution is molecule-independent. We have further found that the electrode separation in the low-conducting state is consistent with a vertical geometry where the molecule is probably bound to apex atoms on each electrode, while the high-conducting state corresponds to junctions with an electrode separation that is smaller than the length of the molecule. These findings have been corroborated by scattering-state density functional theory (DFT)-based conductance calculations, which show that the low-conducting state is associated with a vertical geometry in which the N−Au bonds are aligned with the molecular backbone (and are therefore perpendicular to the π system), while the high-conducting state is associated with a geometry in which the molecule is tilted, resulting in an increased coupling from the electrode to the molecular π system.[15] For the three conjugated molecules in our study, the measured conductance decreases with increasing length, with a decay constant (β) of ∼0.5/Å, suggestive of off-resonant tunneling transport dominated by a π channel. This occurs in spite of the σ nature of the N−Au link bonds in the low-conductance geometry but in agreement with our calculations which indicate that the dominant conducting channel in the low-conductance geometry has π character for the conjugated molecules. The measured conductance for the molecule with broken conjugation (molecule **4**) is much smaller than one would generally expect for a molecule of its length. In this case, our calculations have shown that the dominant conducting channel has σ character throughout the molecule. We attribute this to an interference effect that suppresses the channel with π character in the pyridine rings.

2. Experimental Methods and Results

Molecules **1**, **2**, and **4** were obtained from Sigma-Aldrich and used without further purification, and molecule **3** was synthesized following methods described in the literature.[20] Our measurements were carried out using a home-built STM that has been described in detail previously.[2,21] We repeatedly pulled the STM tip and substrate apart while recording the conductance as a function of junction elongation under constant bias in a 1,2,4-trichlorobenzene (Sigma-Aldrich) solution of these molecules. Figure 1b shows sample traces demonstrating the evolution of the conductance as the junction was stretched in the presence of molecules **1**−**4**. Plateaus in these traces below the quantum of conductance (G_0) occur when a molecule is held between the tip and substrate. Conductance histograms generated from over 20 000 conductance traces for each of the molecules are shown in Figure 1c, where we can see that the double-peak feature is universal to the pyridine linker.[15] Interestingly, the high-conductance peak is less distinct in molecule **4** than in molecules **1**−**3**, a feature that we further discuss below.

In Figure 2a,b, we show two-dimensional (2D) histograms (which preserve displacement information) for molecules **2** and

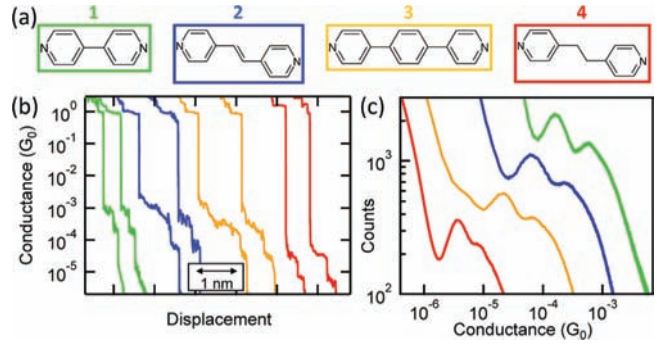

Figure 1. (a) Structures of compounds **1**−**4** studied in this work. (b) Sample conductance traces acquired while the junction was pulled apart at a rate of ∼15 nm/s in the presence of the individual target molecules **1**−**4** under an applied bias of 350 mV. (c) Conductance histograms for molecules **1**−**4**, each constructed from over 20 000 measured traces. Two peaks are clearly visible in each curve and were fit to Lorentzians to determine the peak center positions.

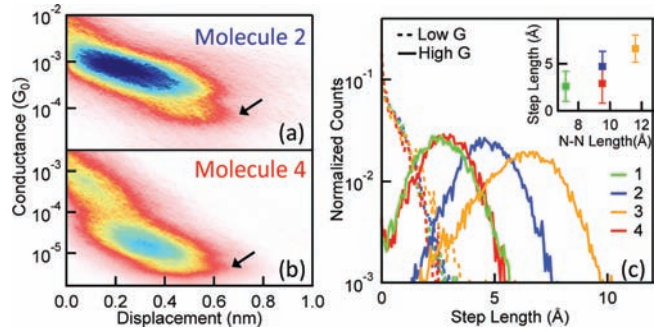

Figure 2. (a, b) 2D conductance histograms for molecules **2** and **4** constructed from all of the measured traces that showed a clearly defined break after the $1G_0$ step; at least 10 000 curves were included in each histogram. The arrows point to the low-conductance regime, which extends to ∼0.7 nm past the G_0 break. (c) Length distributions of the high-conductance (solid lines) and low-conductance (dashed lines) plateaus. Inset: Peak value of the high-conductance plateau length distribution as a function of the molecule N−N length.

(14) Kamenetska, M.; Koentopp, M.; Whalley, A.; Park, Y. S.; Steigerwald, M.; Nuckolls, C.; Hybertsen, M.; Venkataraman, L. *Phys. Rev. Lett.* **2009**, *102*, 126803.
(15) Quek, S. Y.; Kamenetska, M.; Steigerwald, M. L.; Choi, H. J.; Louie, S. G.; Hybertsen, M. S.; Neaton, J. B.; Venkataraman, L. *Nat. Nanotechnol.* **2009**, *4*, 230–234.
(16) Zhou, X. S.; Chen, Z. B.; Liu, S. H.; Jin, S.; Liu, L.; Zhang, H. M.; Xie, Z. X.; Jiang, Y. B.; Mao, B. W. *J. Phys. Chem. C* **2008**, *112*, 3935–3940.
(17) Wang, C. S.; Batsanov, A. S.; Bryce, M. R.; Martin, S.; Nichols, R. J.; Higgins, S. J.; Garcia-Suarez, V. M.; Lambert, C. J. *J. Am. Chem. Soc.* **2009**, *131*, 15647–15654.
(18) Haiss, W.; van Zalinge, H.; Higgins, S. J.; Bethell, D.; Hobenreich, H.; Schiffrin, D. J.; Nichols, R. J. *J. Am. Chem. Soc.* **2003**, *125*, 15294–15295.
(19) Li, Z. H.; Pobelov, I.; Han, B.; Wandlowski, T.; Blaszczyk, A.; Mayor, M. *Nanotechnology* **2007**, *18*, 044018.
(20) Han, Y. F.; Lin, Y. J.; Jia, W. G.; Jin, G. X. *Organometallics* **2008**, *27*, 4088–4097.
(21) Hybertsen, M. S.; Venkataraman, L.; Klare, J. E.; Whalley, A. C.; Steigerwald, M. L.; Nuckolls, C. *J. Phys.: Condens. Matter* **2008**, *20*, 374115.

4 that were generated from more than 10 000 traces.[14,15,22] We generated such 2D histograms using an automated algorithm that identifies the rupture of the quantum point contact in each trace as the origin of the elongation axis. Each data point in a trace is then associated both with a conductance value and a displacement value relative to the G_0 break, and the histogram is generated using logarithmic bins along the conductance (y) axis and linear bins along the elongation (x) axis for image clarity. When thousands of traces are used, a statistically significant plot of conductance as a function of elongation emerges. We can see that both molecules have plateaus that extend out to ~0.6 nm; the conductance is high in the initial stages, and the low-conductance plateau occurs only after ~4 Å of additional junction stretching.

To investigate these trends in more detail, we used an automated algorithm detailed previously[23] to measure the elongation lengths of the conductance plateaus in each trace. We performed this analysis on thousands of traces and generated length distributions of both the high- and low-conductance plateaus for each molecule by identifying plateaus as regions within the conductance traces between two successive drops in conductance.[23] The results are shown in Figure 2c. The inset of Figure 2c shows the peak positions of the high-conductance length distribution plotted against the molecule length. We see that the most frequently observed high-conductance step length increases linearly with molecule N−N distance for molecules **1**−**3**. For molecule **4**, our algorithm misses the initial part of each step, probably because direct tunneling through the broken Au−Au contact dominates at small Au−Au separations. On the other hand, the low-conductance plateaus of all four molecules are shorter than high-conductance plateaus and show no dependence on molecule length. These distributions do not have maxima; they fall off exponentially. The two distinct length scales, one dependent on molecule length and the other length-independent, suggest that at least two separate elongation processes are responsible for the high- and low-conductance plateaus. Atomic rearrangements, such as changes in the nitrogen attachment point or motion of a gold atom on the electrode surface, can explain the high-conductance step lengths and their dependence on molecule length.[14] We hypothesize that all rearrangements in the attachment of the molecule to the gold take place before the low-conductance configuration is established, leaving only bond rupture, which is independent of molecule length, as the main process responsible for low-conductance plateaus.

To test this hypothesis, we measured the conductance as a function of both junction elongation and compression (see the Supporting Information for details). We repeatedly opened and then closed a quantum point contact in a solution of molecules under a constant bias.[15] We determined the distance needed to push the electrodes back together to reestablish a conductance greater than G_0 for a molecular junction in either the high- or low-conductance regime. This push-back distance gives the distance between the gold electrodes in a molecular junction (excluding the length of a gold−gold bond, which is ~3 Å). We can correlate the push-back distance to the average conductance of the gold−molecule−gold configuration. The resulting plot of average conductance as a function of electrode separation for molecule **4** is shown in Figure 3a, together with the original conductance histogram for reference. We observe that junctions within the low-conductance regime are possible only when the push-back distance is ~12 Å (arrow in Figure 3a). Taking into account the length of molecule **4** (the N−N length is 9.5 Å) and the length of the N−Au bond (~2.5 Å), this separation is consistent with a junction geometry in which the molecule is stretched between the electrodes. In Figure 3b, we show histograms of push-back distances in the low-conductance regime for pyridine-terminated molecules of different lengths. The inset plots the peak of each histogram as a function of molecule N−N distance. A linear fit to this data gives a slope less than unity, indicating that on average, the molecular junction has a slight tilt relative to the orientation of the pushing direction. We stress here that this is *not* the same as a local tilt between the N−Au bond orientation and the plane of the pyridine ring, which is responsible for increased π coupling in the high-conductance region. We note further that the correlation between electrode distance in the low-conductance regime and molecule length holds for both conjugated (**1**−**3**) and nonconjugated (**4**) molecules in our sample.

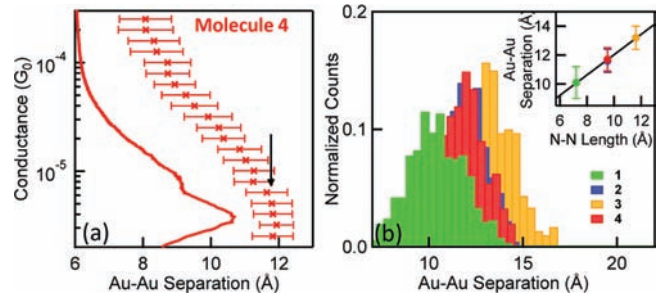

Figure 3. (a) Data points showing average junction conductance during the hold portion of each trace with molecule **4** (see Figure S1 in the Supporting Information) plotted against average electrode separation as determined by measuring the pushing distance required to close the contact. For reference, the conductance histogram from Figure 1c is reproduced. The arrow shows the low-conductance configuration where the push-back distance is ~1.2 nm. The high-conductance geometry is realized at shorter gold−gold distances. (b) Histograms of measured push-back distances for all four molecules in the low-conductance geometry. Inset: Peak position of the push-back distance histogram as a function of molecule length with a linear fit to the data.

These results agree well with our previous work on bipyridine−Au junctions, where we inferred that the conductance is low in the vertical geometry where the N−Au bond is perpendicular to the π system and high when the molecule is tilted (e.g., when the Au point contact is first broken) to allow coupling of the N−Au bond to the π system.[15] These conclusions are corroborated by the 2D histograms in Figure 2b, where we see that the conductance after the G_0 rupture starts in the high-conductance configuration, and only after further elongation of the junction by a molecule-dependent length can the low-conductance geometry be accommodated.[15] The bimodal conductance histogram observed here can be explained by considering the evolution and rearrangement of contact structure upon junction elongation: as the contacts are pulled apart, molecules initially trapped in the junction at acute angles may abruptly transition from one binding site to another before reaching a vertical configuration and then breaking.

We now focus on the conductance values determined by our measurements, which are plotted in Figure 4 as a function of molecule length. These conductance values were determined by fitting Lorentzians to the high- and low-conductance peaks in the data shown in Figure 1c. We see that the values for the

(22) Martin, C. A.; Ding, D.; Sorensen, J. K.; Bjornholm, T.; van Ruitenbeek, J. M.; van der Zantt, H. S. J. *J. Am. Chem. Soc.* **2008**, *130*, 13198–13199.
(23) Quek, S. Y.; Venkataraman, L.; Choi, H. J.; Louie, S. G.; Hybertsen, M. S.; Neaton, J. B. *Nano Lett.* **2007**, *7*, 3477–3482.

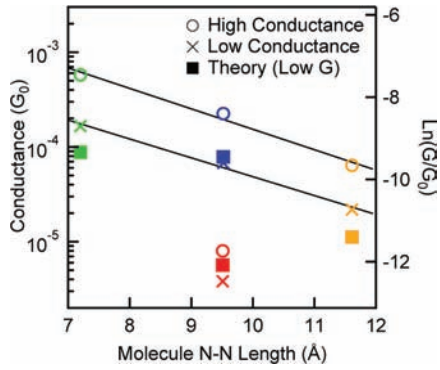

Figure 4. Conductance values determined by fitting Lorentzians to the peaks of the conductance histograms shown in Figure 1 for the low-conductance (×) and high-conductance (○) peaks for molecules **1**−**4**. Linear fits to the data on a semilog plot (solid lines) yielded a value of ∼0.5 Å^{-1} for the constant β in $G \sim e^{-\beta L}$. Calculated conductances for all molecules in a vertical geometry are shown with ■ symbols.

conjugated molecules in our sample (molecules **1**−**3**) decay exponentially as a function of molecule length, following the general relation $G \sim e^{-\beta L}$, where L is the molecule N−N length and β is the tunneling decay factor, while the conductance for molecule **4**, where the conjugation is broken by the intervening, saturated $(CH_2)_2$ unit, is orders of magnitude smaller. We found that $\beta \approx 0.5$ Å^{-1} for both the high- and low-conductance peaks in molecules **1**−**3**, in agreement with previously measured values for polyphenyl molecules.[24,25] While the β value is expected to be sensitive to the Fermi level alignment within the HOMO−LUMO gap of the different systems,[26−29] the relatively small value of β found here strongly suggests that the dominant conductance channel in the conjugated bipyridines has π character, despite the facts that the bonding of the molecule to the gold occurs through the N σ orbital and that in the low-conductance state, the N−Au bond is almost perpendicular to the π system.

3. Theoretical Methods and Results

To investigate in detail the conducting channels in the different molecules for the low-conductance geometry,[30−33] we computed the conductance and zero-bias transmission with a DFT-based scattering state approach[15,27,34] using the generalized gradient approximation,[35] as implemented in the SIESTA code.[36] A self-energy correction,[16,24] including electrode polarization effects on the molecular orbital (MO) energy levels in the junction,[37] was then added to the Hamiltonian, from which the scattering states were obtained in a one-shot calculation.[27] We modeled the low-conductance state with a vertical geometry (Figure 5a) using periodic boundary conditions parallel to the Au surface (16 Au atoms per layer). For all four molecules, a three Au atom motif was used to represent the tip of each electrode, with the N bonded to one of the Au atoms of the motif at an atop site. These binding sites were located on top of four Au layers on either side of the molecule, which were then extended to infinity on either side of the junction to simulate open boundary conditions. The transmission was converged with a 4 × 4 $\mathbf{k}_{||}$ mesh. The conductance was computed as $G = G_0 \sum_{\mathbf{k}_{||}} \mathrm{Tr}(\mathbf{t}^\dagger \mathbf{t})$, where the elements t_{ij} of the matrix $\mathbf{t}$ are the transmission amplitudes from incoming channels i to outgoing channels j at a given $\mathbf{k}_{||}$ point at the Fermi energy E_F. Our calculated conductance values agree well with the measured low-conductance values for all of the molecules (as plotted in Figure 4), falling within the low-conductance histogram peaks shown in Figure 1c. The transmission plots in Figure 5b show that for all molecules considered, the lowest unoccupied MO (LUMO) has π* character in the pyridine rings and is the frontier orbital closest to E_F. The narrow transmission peak widths (0.1−0.3 eV) are consistent with relatively weak coupling between the π system and the Au s−p band in the vertical geometry.[15]

To analyze the character of the wave functions dominating the conductance at E_F, we diagonalized the transmission matrix $\mathbf{t}^\dagger\mathbf{t}$ to obtain the eigenchannels at each $\mathbf{k}_{||}$ point.[38] Each eigenchannel at each $\mathbf{k}_{||}$ point can in principle contribute to the total transmission at E_F; the sum of these contributions gives the total conductance. We found that in practice, only ∼2 eigenchannels at each $\mathbf{k}_{||}$ point make non-negligible contributions for the junctions studied here. By visualizing the wave functions for all of the eigenchannels with nonzero transmission at E_F (the "conducting eigenchannels"), we found that for molecules **1**−**3**, the total conductance is dominated by eigenchannels consisting of the molecular π* LUMO coupled to Au p states at the binding site (see SI Figure S2a,d). A small residual contribution consists of σ orbitals coupled to Au s states, with the eigenchannel wave function resembling the frontier orbitals of the gas-phase molecule bonded to a single Au atom at each N in the same binding configuration (Au−N bond perpendicular to the π system) (e.g., SI Figure S2b,e). To quantify the π (or π*) contributions to the conductance, we summed the transmission from each conducting eigenchannel possessing nodes in the planes of the pyridine rings. In this case, the lobes of the wave functions in the pyridine rings clearly indicate π* LUMO character. The remaining conducting eigenchannels have σ character, as described above. From this analysis, we found that the LUMO (π*) contributes ∼75% of the total conductance for bipyridine, with the remainder having σ character. For molecules **2** and **3**, the π* contribution is greater than 90%.

In contrast, however, for molecule **4**, none of the conducting eigenchannels have nodes in the planes of the pyridine rings. About 80% of the conductance can be attributed to molecular σ orbitals, as described above for molecules **1**−**3** (SI Figure S2b,e). The remaining conductance comes from states that are a combination of σ and π orbitals but bear no clear resemblance

(24) Beebe, J. M.; Engelkes, V. B.; Miller, L. L.; Frisbie, C. D. *J. Am. Chem. Soc.* **2002**, *124*, 11268–11269.
(25) Venkataraman, L.; Klare, J. E.; Nuckolls, C.; Hybertsen, M. S.; Steigerwald, M. L. *Nature* **2006**, *442*, 904–907.
(26) Tomfohr, J. K.; Sankey, O. F. *Phys. Rev. B* **2002**, *65*, 245105.
(27) Quek, S. Y.; Choi, H. J.; Louie, S. G.; Neaton, J. B. *Nano Lett.* **2009**, *9*, 3949–3953.
(28) Wang, J. G.; Prodan, E.; Car, R.; Selloni, A. *Phys. Rev. B* **2008**, *77*, 245443.
(29) Prodan, E.; Car, R. *Phys. Rev. B* **2009**, *80*, 035124.
(30) Stadler, R.; Thygesen, K. S.; Jacobsen, K. W. *Phys. Rev. B* **2005**, *72*, 241401.
(31) Wu, X. J.; Li, Q. X.; Huang, J.; Yang, J. L. *J. Chem. Phys.* **2005**, *123*, 184712.
(32) Bagrets, A.; Arnold, A.; Evers, F. *J. Am. Chem. Soc.* **2008**, *130*, 9013–9018.
(33) Li, Z. L.; Zou, B.; Wang, C. K.; Luo, Y. *Phys. Rev. B* **2006**, *73*, 075326.
(34) Choi, H. J.; Cohen, M. L.; Louie, S. G. *Phys. Rev. B* **2007**, *76*, 155420.
(35) Perdew, J. P.; Burke, K.; Ernzerhof, M. *Phys. Rev. Lett.* **1996**, *77*, 3865–3868.
(36) Soler, J. M.; Artacho, E.; Gale, J. D.; Garcia, A.; Junquera, J.; Ordejon, P.; Sanchez-Portal, D. *J. Phys.: Condens. Matter* **2002**, *14*, 2745–2779.
(37) Neaton, J. B.; Hybertsen, M. S.; Louie, S. G. *Phys. Rev. Lett.* **2006**, *97*, 216405.
(38) Brandbyge, M.; Sorensen, M. R.; Jacobsen, K. W. *Phys. Rev. B* **1997**, *56*, 14956–14959.

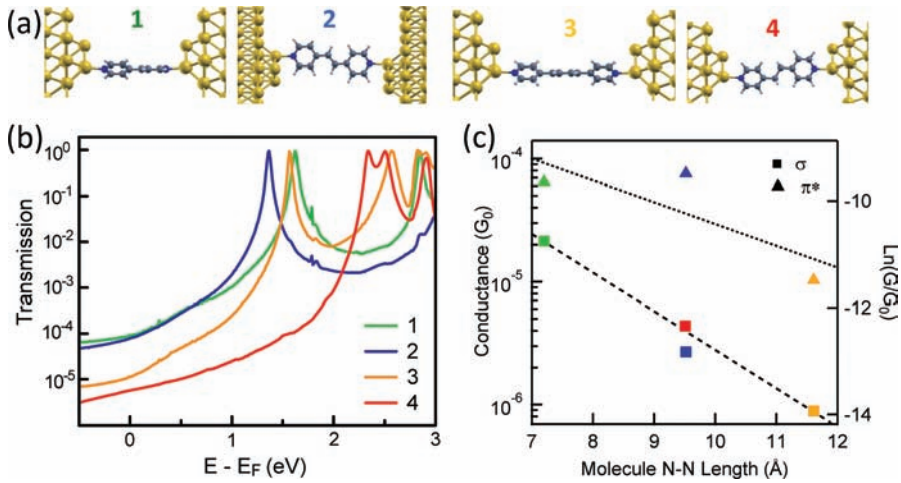

Figure 5. (a) Optimized structures of the junctions for molecules **1**−**4**. Gold, gray, blue, and white circles represent Au, C, N, and H, respectively. The molecules are bound via N to an atop site of a Au trimer (three Au atoms) on Au(111). (b) Transmission plots. (c) Plot of the logarithm of molecular π^* and σ contributions to the conductance as functions of the molecule length. The π^* contribution to the conductance of molecule **4** has been omitted because it is negligible on the scale of the plot.

to the LUMO or LUMO+1 state (SI Figure S2c,f). The fact that the LUMO does not contribute significantly to the conductance at E_F is consistent with the sharp decrease in transmission below the LUMO transmission peak for molecule **4**, as shown in Figure 5b. The π states on the two pyridine groups in molecule **4** are weakly coupled through the intervening $(CH_2)_2$ linkage, resulting in a closely spaced π^* doublet (LUMO and LUMO+1). The sharp decrease in transmission is likely a result of destructive interference between the closely spaced LUMO and LUMO+1 resonances, as the transmission peaks do not fit well to a simple sum of two Lorentzians (SI Figure S3d). This is in contrast to the nearly Lorentzian line shapes observed for the isolated LUMO transmission peaks in molecules **1**−**3** (SI Figure S3a−c).

The fact that σ MOs can contribute to the conductance at E_F may seem surprising, since the π^* LUMO is the MO closest to E_F (SI Table 1). However, the Au states at E_F are predominantly s-like. As discussed previously,[15] in the low-conductance vertical geometry, s states are orthogonal to the π system and cannot couple directly to the LUMO. Therefore, the LUMO contributes to conductance at E_F only through coupling to local Au p states, which make a small contribution to the Au density of states at E_F. In contrast, σ MOs can couple strongly to the Au s states at E_F. In Figure 5c, we show the π^* and σ contributions to the conductance as functions of the length of the molecule. The decrease in π^*-derived conductance with increasing length correlates well with the experimental values, yielding a β value of ~0.4/Å. In contrast, the σ contribution decreases with a β of ~0.7/Å. This indicates that the σ contribution to the conductance in molecule **4** is in fact similar to that in other molecules of the same length (specifically molecule **2**), while its π^* contribution to the conductance is suppressed by the destructive interference described above, resulting in a significantly smaller total conductance for **4**. Finally, we noted in Figure 1c that the high-conductance peak is less distinct for molecule **4** than for **1**−**3**. Since the low- and high-conductance regimes respectively result from the smaller and larger coupling between the Au states and the π system in the vertical and tilted geometries, it is likely that the relatively smaller contribution of the LUMO in molecule **4** makes the two conductance regimes less distinct.

4. Conclusions

We have employed a novel pulling−pushing break-junction procedure to investigate the relationship between metal−molecule−metal junction geometry and junction conductance for a series of pyridine-terminated molecules having various lengths and conjugation. We have found that the double-peak conductance signature is universal for pyridine-linked molecules and is due to the existence of two distinct binding geometries. By pushing on molecular junctions, we identified the electrode separation of each conductance state. Lower conductance occurs when the N−Au donor−acceptor bond is along the molecular backbone; in this configuration, the distance between the gold electrodes depends on the length of the molecule in the junction. Finally, we have employed first-principles calculations to show that conductance is dominated by transport through the π system in the conjugated molecules, in agreement with the relatively small β value observed in the experiments. The predicted conductance values are in excellent agreement with experimental values.

Acknowledgment. This work was supported in part by the Nanoscale Science and Engineering Initiative of the NSF (Awards CHE-0117752 and CHE-0641532), the New York State Office of Science, Technology, and Academic Research (NYSTAR), and the Packard Foundation (M.K. and L.V.). Portions of this work were performed at the Molecular Foundry, Lawrence Berkeley National Laboratory, and were supported by the U.S. Department of Energy, Office of Science, Office of Basic Energy Sciences, under Contract DE-AC02-05CH11231. This work was supported in part by the U.S. Department of Energy, Office of Basic Energy Sciences, under Contract DE-AC02-98CH10886 (M.S.H.). H.J.C. acknowledges support from NRF of Korea (Grant 2009-0081204).

Supporting Information Available: Experimental and data analysis procedures, SI Figures S1−S3, and SI Table 1. This material is available free of charge via the Internet at http://pubs.acs.org.

JA1015348